Nanoscale

PAPER

View Article Online
View Journal | View Issue

# Thermal stability of $Mn^{2+}$ ion luminescence in Mn-doped core–shell quantum dots†

Cite this: *Nanoscale*, 2014, **6**, 300

Xi Yuan,[ab] Jinju Zheng,[c] Ruosheng Zeng,[d] Pengtao Jing,[a] Wenyu Ji,[a] Jialong Zhao,*[ae] Weiyou Yang*[c] and Haibo Li*[e]

Received 15th August 2013
Accepted 2nd October 2013

DOI: 10.1039/c3nr04319c

www.rsc.org/nanoscale



The thermal stability of luminescence is important for the application of quantum dots (QDs) in light-emitting devices. The temperature-dependent photoluminescence (PL) intensities and decay times of Mn-doped ZnS, ZnSe, and ZnSeS alloyed core–shell QD films were studied in the temperature range from 80 to 500 K by steady-state and time-resolved PL spectroscopy. It was found that the thermal stability of Mn-doped QD emissions was significantly dependent on the shell thickness and the host bandgap, which was higher than that of workhorse CdSe QDs. Nearly no PL quenching took place in Mn:ZnS QDs with a thick ZnS shell, which kept a high PL quantum yield (QY) of ~50% even at 500 K; and the thermally stable PL was also observed in highly luminescent Mn:ZnSe and Mn:ZnSeS QDs with a quenching temperature over 200 °C. Further, the stability of Mn-doped QDs with different shell thickness at high temperature was also examined through heating–cooling cycling experiments. The PL quenching in the thick shell-coated Mn-doped QDs was almost totally recovered. The PL quenching mechanisms of the $Mn^{2+}$ ion emissions were discussed.

## 1. Introduction

Colloidal semiconductor quantum dots (QDs) have drawn considerable attention for their size- and composition-tunable photoluminescence (PL), rich electronic structures, and flexible solution processability.[1–4] Doping transition metal ions, *e.g.* $Mn^{2+}$, into semiconductor QDs introduces new optical, electronic, and magnetic properties to the host nanocrystals, exhibiting extensive applications in solar energy conversion,[5] electroluminescent devices,[6,7] and biological labels.[8,9] In comparison with the current workhorse CdSe QDs, the $Mn^{2+}$ ion doped QDs usually contain no heavy metal ions, and have advantages of no self-quenching due to the large Stokes shift,[8–10] and suitability for applications where high density emitters are required, such as solid state lighting and lasers. In recent years, nearly pure and highly efficient (above 50%) Mn dopant emission has been achieved in Mn:ZnS,[11] Mn:ZnSe,[12,13] and Mn:ZnSeS QDs,[14] moreover, narrow and widely tunable Mn emission from deep green to deep red has been observed.[15] These properties make the heavy metal free Mn-doped QDs relevant to be used in light-emitting devices (LEDs). As we know, the luminescence efficiency of QDs is a key factor to determine the performance of LEDs. However, the luminescence efficiencies of Mn-doped QDs were reported to be strongly temperature-dependent, and generally decrease at elevated temperature.[16–19] And yet, for most optical devices of QDs, the thermal effects are inevitable and the working temperature is higher than room temperature due to heat dissipation of the QDs themselves.[20] The working temperature is even up to 450 K, when the QDs are applied as color converters in warm-white LEDs.[21] Therefore, the QDs with a high luminescence efficiency and an improved thermal stability at high temperature are urgently needed for their ultimate commercialization of QD luminescent devices.

The studies of the thermal stability of Mn-doped QDs were almost focused on the cryogenic temperature range of 5–300 K in early works. In this temperature region, serious thermal quenching of $Mn^{2+}$ ion emissions observed by many groups[16–19] was generally attributed to the thermal activation to the defect states; besides, temperature antiquenching due to thermal release of delocalized carriers to $Mn^{2+}$ ions was also

[a]*State Key Laboratory of Luminescence and Applications, Changchun Institute of Optics, Fine Mechanics and Physics, Chinese Academy of Sciences, 3888 Eastern South Lake Road, Changchun 130033, China. E-mail: zhaojl@ciomp.ac.cn; Tel: +86-431-86176313*

[b]*University of Chinese Academy of Sciences, Beijing 100039, China*

[c]*Institute of Materials, Ningbo University of Technology, Ningbo 315016, China. E-mail: weiyouyang@tsinghua.org.cn; Tel: +86-574-87080966*

[d]*School of Chemistry and Material Science, Guizhou Normal University, Guiyang 550001, China*

[e]*Key Laboratory of Functional Materials Physics and Chemistry of the Ministry of Education, Jilin Normal University, Siping 136000, China. E-mail: lihaibo@jlnu.edu.cn; Tel: +86-434-3290232*

† Electronic supplementary information (ESI) available: The synthesis of Mn:ZnS, Mn:ZnSe, and Mn:ZnSeS QDs. TEM images of MnS core and Mn-doped ZnSe, $ZnSe_{0.73}S_{0.27}$, and $ZnSe_{0.22}S_{0.78}$ QDs. Temperature-dependent PL intensities and lifetimes of Mn:ZnSe QDs. Temperature-dependent PL spectra of Mn:$ZnSe_{0.73}S_{0.27}$, Mn:$ZnSe_{0.22}S_{0.7}$, and CdSe/CdZnS/ZnS core–shell QDs. Temperature-dependent integrated PL intensities of Mn:ZnS (4.5 ML ZnS), Mn:$ZnSe_{0.73}S_{0.27}$, Mn:$ZnSe_{0.22}S_{0.7}$, and CdSe/CdZnS/ZnS core–shell QDs in heating–cooling circle experiments. See DOI: 10.1039/c3nr04319c

observed.[22,23] The two competing factors determined the ultimate temperature dependent PL behaviors, which could be controlled by the particle size and the shell structure.[22,24] Above room temperature, only a few reports were relative to luminescence properties of Mn-doped QDs. Chen reported that the emission in Mn:ZnS QDs was quenched completely at 140 °C,[17] while the Mn:ZnSe QDs with little temperature quenching (PL spectra recorded *in situ*) have been achieved by Peng's group.[13] However, previous reports have not provided the systemic research on the thermal stability of luminescence for Mn-doped QDs against the thermal quenching, the thermally induced structural changes, and the intrinsic PL quenching mechanisms under high temperature conditions. Hence, the method to improve the high-temperature thermal stability of $Mn^{2+}$ ion emission is still unclear. Moreover, the stability of Mn-doped QDs at elevated temperature is significant for the QD applications in optical devices. Therefore, better understanding of the PL quenching mechanisms and improving the thermal stability under high temperature conditions for Mn-doped QDs are highly desired.

In this work, we systematically investigated the thermal behaviours of $Mn^{2+}$ ion emissions in MnS–ZnS, MnSe–ZnSe, and MnSe–ZnSeS alloyed core–shell QD films by the temperature-dependent steady-state and time-resolved PL spectroscopy from 80 to 500 K. The PL quenching mechanisms were explored by comparing the temperature-dependent PL intensities and PL lifetimes of the Mn-doped QDs with varying the shell thickness and host material. Then, the effects of the shell and host bandgap of the Mn-doped core–shell QDs on the thermal stability of $Mn^{2+}$ ion emissions were discussed. Further, the stability of the QDs against the thermal degradation of the luminescence performance was examined by heating–cooling cycling experiments.

## 2. Experimental section

### 2.1 Sample preparation

The Mn-doped ZnS, ZnSe, and ZnSeS alloyed core–shell QDs used in this experiment were synthesized *via* a nucleation-doping strategy similar to our previous works.[12,14,22] Briefly, a preformed MnS or MnSe nanocrystal core was initially coated with a ZnS, ZnSe, or ZnSeS shell, and then the doping was achieved by diffusion of $Mn^{2+}$ ions from the core into the shell at elevated temperature (above 220 °C), so the shell also acted as the host for $Mn^{2+}$ ions. The details of the QD synthesis are described in the ESI.† The Mn-doped QDs were collected by dispersing into chloroform solution for further optical measurements and film sample preparation. The film samples used for temperature dependent PL spectra and PL decay measurements were fabricated by dropping the Mn-doped QDs on silicon wafer substrates.

### 2.2 Experimental setup

The absorption spectra were recorded by a U-3900 UV-VIS scanning spectrophotometer (Hitachi). Steady-state PL spectra, PL QY, and time-resolved PL spectra were measured by a Horiba Jobin Yvon Fluromax-4P with a QY accessory and a time-correlated single-photon counting (TCSPC) spectrometer. The continuous excitation source was a 150 W ozone-free xenon arc-lamp and a pulsed xenon lamp was utilized as the excitation source for the PL decay measurement. The size of the QDs was measured by a JEM-2100F transmission electron microscope (TEM). The energy dispersive X-ray spectroscopy (EDS) for the elemental analysis of the inorganic QDs was measured by using a Hitachi S-4800 scanning electron microscope. The film samples were mounted in a Janis VPF-800 vacuum liquid nitrogen cryostat with a controllable temperature region from 80 to 500 K, during the entire measurement.

## 3. Results and discussion

UV-visible absorption and PL spectra of MnS–ZnS core–shell QDs with different ZnS shell thicknesses in chloroform solution are shown in Fig. 1a. The core–shell QDs can also be called Mn:ZnS QDs because the shells also act as the host for Mn dopants.[13] The thicknesses of the shells are estimated to be about 3.4, 4.5 and 6.4 monolayers (MLs), based on the TEM images of the MnS core (Fig. S1a, ESI†) and MnS–ZnS core–shell (Fig. 1b–d) QDs, and one monolayer thickness of 0.31 nm to ZnS materials.[25] As seen in Fig. 1a, a large Stokes shift of about 270 nm (1.77 eV) is observed due to the significant energy differences between the bandgap of the host semiconductor and the energy of the $Mn^{2+}$ ion $^4T_1$ to $^6A_1$ internal d–d transition. The PL QY of the MnS–ZnS core–shell QDs increases monotonously from 14% to 53%, through growing the ZnS shell around the MnS core, passivating the surface trap states.

The left of Fig. 2 shows the temperature-dependent PL spectra of Mn:ZnS QDs with different shell thickness, recorded in the temperature range from 80 to 500 K (heating temperature

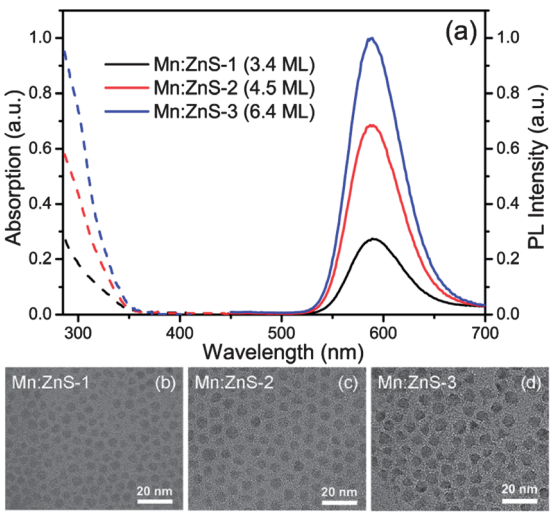


Fig. 1 (a) UV-visible absorption (dashed lines) and PL (solid lines) spectra of MnS–ZnS core–shell QDs with shell thicknesses of 3.4 (Mn:ZnS-1, black lines), 4.5 (Mn:ZnS-2, red lines), and 6.4 MLs (Mn:ZnS-3, blue lines). The excitation wavelength is 320 nm. TEM images of Mn:ZnS-1 (b), Mn:ZnS-2 (c), and Mn:ZnS-3 (d) QDs.

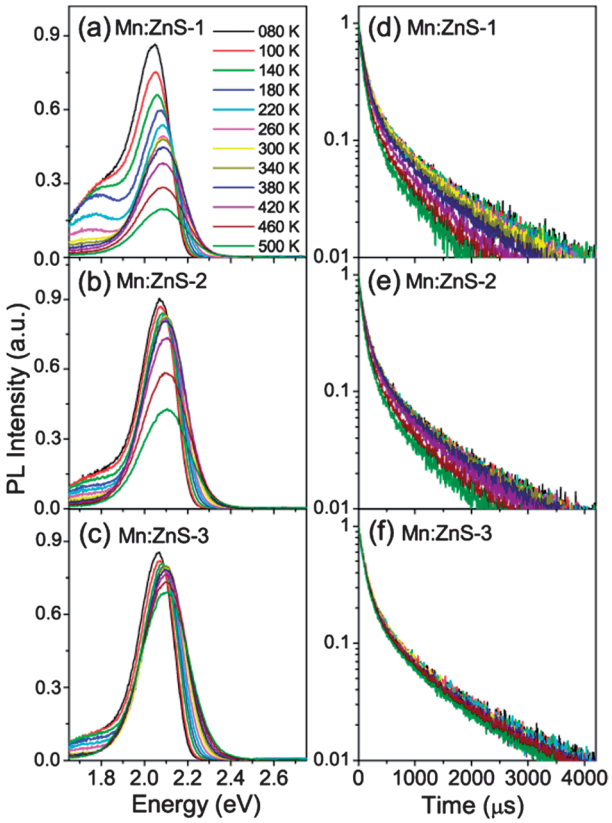


Fig. 2 PL spectra (left) and decay curves (right) of MnS–ZnS core–shell QDs with shell thicknesses of 3.4 (a and d), 4.5 (b and e), and 6.4 MLs (c and f) at different temperatures from 80 to 500 K, under excitation at 280 nm.

over 500 K may induce the loss of capping ligands). As seen in Fig. 2a, the PL intensity of the thin shell (3.4 MLs) QDs quickly drops as the temperature increases. This means that there are a large amount of the nonradiative traps present on the surface of thin shell QDs, inducing strong thermal quenching. The PL intensity of medium shell (4.5 MLs) QDs almost keeps constant when temperature varies from 80 to 380 K, and decreases with increasing temperature from 420 to 500 K, as shown in Fig. 2b; resulting from that the surface nonradiative recombination centers are efficiently passivated as the shell thickness increases. Further, as seen in Fig. 2c, it is excitingly found that almost no PL quenching takes place from 80 to 420 K, and only a little PL quenching occurs as the temperature rises above 460 K in the thick shell (6.4 MLs) QDs, which means that the nonradiative recombination is significantly suppressed. This suggests that our Mn:ZnS QDs with a thick shell can keep high PL QY (~50%) even at the high temperature range of 300–500 K, which means that the Mn:ZnS QDs can sufficiently satisfy the requirements (great thermal stability and high PL QY) for the applications in luminescence devices. In addition, besides the $Mn^{2+}$ ion emission at about 2.1 eV, the surface trap PL at the low-energy side related to the defect in ZnS nanoparticles[17] is observed, which can be eliminated with growing the ZnS shell around the MnS core, indicating that the surface defect states are efficiently passivated.

It is well known that the $Mn^{2+}$ ion emission is due to energy transfer from the exciton in host to the $Mn^{2+}$ ions.[26,27] Therefore, the PL QY of $Mn^{2+}$ ions ($QY_{Mn}$) is determined by both the energy transfer efficiency ($\Phi_{ET}$) and $Mn^{2+}$ ion emission efficiency ($\Phi_{Mn}$), which can be expressed as:[25] $QY_{Mn} = \Phi_{ET} \times \Phi_{Mn}$. The energy transfer process (a few to tens of picoseconds) is significantlyly faster than the $^4T_1$ to $^6A_1$ transition process (milliseconds) of $Mn^{2+}$ ions,[26–29] thus, the PL decay curves can only reflect the $Mn^{2+}$ ion recombination process. Besides, the PL decay lifetime of $Mn^{2+}$ ion emissions ($\tau_{Mn} = 1/(k_r^{Mn} + k_{nr}^{Mn})$, $k_r^{Mn}$ and $k_{nr}^{Mn}$ are the radiative and nonradiative decay rate constant of $Mn^{2+}$ ions) is related to the $Mn^{2+}$ ion emission efficiency $\Phi_{Mn} = k_r^{Mn}/(k_r^{Mn} + k_{nr}^{Mn})$,[25] therefore, we can use $\tau_{Mn}$ to reflect $\Phi_{Mn}$. To better understand the different thermal quenching issues in the Mn:ZnS QDs with various shell thicknesses, we measure their luminescence decay curves at different temperatures (80–500 K) shown in the right of Fig. 2. The PL recombination dynamics becomes faster at higher temperature, and the largest, medium, and smallest changes in PL decay with increasing temperature were observed in 3.4, 4.5, and 6.4 ML ZnS shell coated Mn:ZnS QDs, respectively. We analyzed the PL decays by a bi-exponential function with two time components ($\tau_i$) and weights ($A_i$). The amplitude-weighted lifetimes were obtained by a relation $\tau_{av} = (A_1\tau_1 + A_2\tau_2)/(A_1 + A_2)$.

Both the temperature-dependent integrated PL intensities (normalized at 80 K) and lifetimes are plotted in Fig. 3. The PL intensity drops about 70% for thin shell QDs, 40% for medium shell QDs, and only about 10% for thick shell QDs, after heating up to 500 K, compared to that at 80 K. This suggests that the thin shell QDs with a low PL QY are more sensitive to the

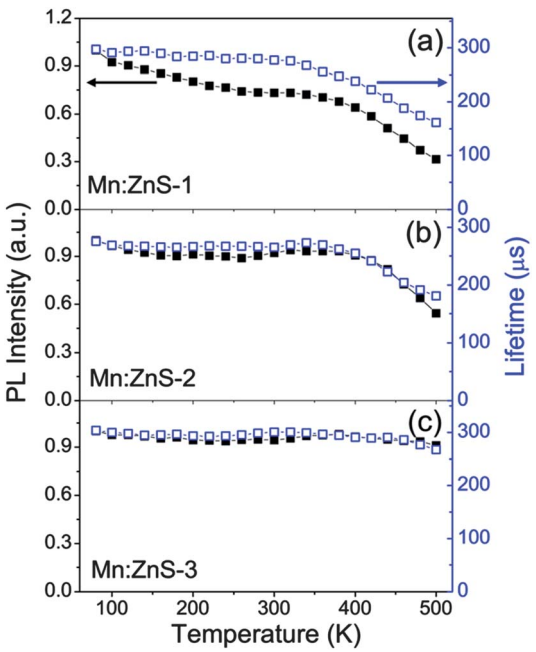


Fig. 3 Temperature dependence of the integrated PL intensities (black solid squares) and decay times (blue open squares) of $Mn^{2+}$ ions in MnS–ZnS core–shell QDs with shell thicknesses of 3.4 (a), 4.5 (b), and 6.4 MLs (c).

temperature than the thick shell QDs with a high PL QY. We know that both the energy transfer efficiency ($\Phi_{ET} = k_{ET}/(k_r^{QD} + k_{nr}^{QD} + k_{ET})$, $k_{ET}$ is the energy transfer rate constant, $k_r^{QD}$ and $k_{nr}^{QD}$ are the radiative and nonradiative decay rates (without energy transfer) of the host)[25] and $Mn^{2+}$ ion emission efficiency ($\Phi_{Mn}$) are dependent on the nonradiative decay rates ($k_{nr}^{QD}$, $k_{nr}^{Mn}$), which will become fast with increasing the temperature. Hence, using a thick shell to passivate the surface trap states and decrease the density of nonradiative recombination centers can effectively improve the PL QY and thermal stability of Mn-doped QDs. On the other hand, increasing the shell thickness can also make the Mn dopant centers sufficiently far away from the surface, thus the thermally activated carries trapping by surface states cannot effectively affect the $Mn^{2+}$ ion emission. Moreover, we observed a similar trend in the PL intensities and lifetimes with the temperature, present in medium and thick shell QDs, indicating that the thermal quenching is mainly due to the decrease of $\Phi_{Mn}$. Meanwhile, the PL intensity drops faster than the PL lifetime with increasing temperature in thin shell QDs, which reveals both the decrease of $\Phi_{Mn}$ and drop of $\Phi_{ET}$ are responsible for the PL thermal quenching. The $\Phi_{Mn}$ significantly impacts all three kinds of Mn:ZnS QDs, and $\Phi_{ET}$ only partially refers to the thin shell QDs. This issue may be attributed to the larger energy transfer rate ($k_{ET} \sim 10^{11}$ $s^{-1}$) than $Mn^{2+}$ ion radiative rate ($k_r^{Mn} \sim 10^3$ $s^{-1}$).[26–29] Therefore, we could amend the thermal stability of $Mn^{2+}$ ion emission in QDs by increasing the shell thickness, decreasing the density of nonradiative recombination centers, making the $Mn^{2+}$ ions sufficiently far away from the surface traps, and perhaps enhancing the energy transfer rate or radiative rate of $Mn^{2+}$ ions.

It was noted that serious PL thermal quenching occurred for Mn-doped QDs reported before.[16–19] These results are vastly different from our Mn:ZnS QDs. Here, we noticed that, in the early works, the Mn-doped QDs generally showed low PL QY, suffering from the low doping yield and/or a significant portion of the doped ions near the surface of the QDs.[30,31] The low doping yield means the slow energy transfer process[28] and the doped ions near the surface make the $Mn^{2+}$ ion emission efficiency susceptible to the temperature, therefore the strong thermal quenching presented in these Mn-doped QDs.

Besides the wide bandgap semiconductor ZnS, the ZnSe semiconductor is also a commonly used, heavy metal free host material for Mn dopants, and the Mn:ZnSe QDs have been used in solid state lighting.[32,33] However, there are no reports about the thermal stability of Mn:ZnSe QD films at high temperature. The PL spectra and decay curves at different temperatures (80–500 K) of Mn:ZnSe (MnSe–ZnSe core–shell) QD films are shown in Fig. 4. The shell thickness of the Mn:ZnSe QDs with a PL QY of ~56% is estimated to be 6.2 MLs from the TEM (Fig. S1b, ESI†). As seen in Fig. 4, the PL intensity of the Mn:ZnSe QDs shows little change with increasing the temperature from 80 to 380 K and quickly decreases at a temperature above 380 K; simultaneously, the PL decay exhibits the similar trend. It is interesting to see that, in Fig. 2c and 4, both Mn:ZnS and Mn:ZnSe QDs synthesized by the nucleation-doping strategy[12,22] possess high PL QY (above 50%) and thick shell (above 6 MLs), however, Mn:ZnS QDs can keep the high PL QY

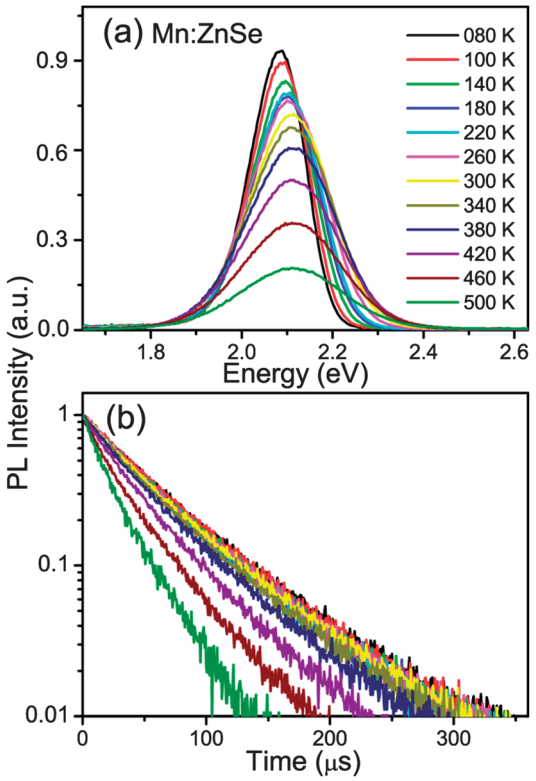


Fig. 4 PL spectra (a) and decay curves (b) of Mn:ZnSe QDs at different temperatures from 80 to 500 K, under excitation at 280 nm.

at high temperature, while the PL QY of Mn:ZnSe QDs rapidly drops with increasing temperature. To better understand this issue, the temperature-dependent integrated PL intensities and lifetimes of Mn:ZnSe QDs are plotted in the ESI (Fig. S2).† The similar trend for the PL intensity and lifetime indicates that the decrease of $\Phi_{Mn}$ should be responsible for the thermal quenching of Mn:ZnSe QDs.

In general, thermal quenching behavior in QDs is attributed to multiphonon relaxation and thermally activated nonradiative recombination processes.[19,20,34] The large $^4T_1$–$^6A_1$ energy gap combines with the low phonon energies provided by ZnSe semiconductor lattices, at least 60 vibrational quanta are needed, hence the multiphonon relaxation is not expected to be the reason for the thermal quenching of Mn:ZnSe QDs. The thermally activated nonradiative recombination process induces the PL quenching by thermal escape of carriers from the luminescent center. For QDs, this process is generally viewed as the thermally activated escape of carriers to the trap state.[20,35] Moreover, in phosphors, it also involves thermally activated photoionization from the localized dopant excited state to the host conduction band.[36,37] In our work, the Mn:ZnS and Mn:ZnSe QDs exhibit similar PL QY and shell thickness, and are both synthesized by the nucleation-doping strategy,[12,22] which indicates that the nature and location of the defects or traps should be similar. Therefore, their difference in thermal stability is not supposed to just arise from the thermally activated escape of carriers to trap states. The thermal quenching of Mn:ZnSe QDs should probably be caused by the

photoionization from the localized dopant excited state to the host conduction band, because the bandgap of ZnSe (2.7 eV) is smaller than that of ZnS (3.7 eV). Based on this viewpoint, the host with a larger bandgap is expected to exhibit better PL thermal stability. So we examined the temperature-dependent PL spectra of Mn-doped $ZnSe_{0.73}S_{0.27}$ and $ZnSe_{0.22}S_{0.78}$ QDs (Fig. S3, ESI†), with the bandgap of 3.1 and 3.3 eV estimated from the absorption spectra, respectively, which were larger than that of ZnSe. The PL QY is 51% and 46%, and the shell thickness is 6.3 and 5.2 MLs (Fig. S1c and d, ESI†) for $Mn:ZnSe_{0.73}S_{0.27}$ and $Mn:ZnSe_{0.22}S_{0.78}$ QDs, respectively. Their integrated PL intensities (normalized at 300 K) as a function of temperature are plotted in Fig. 5; for comparison, the PL intensities of Mn:ZnSe and Mn:ZnS QDs at different temperature are also shown in this figure.

As seen in Fig. 5, with raising the host bandgap, the Mn:ZnSe, $Mn:ZnSe_{0.73}S_{0.27}$, $Mn:ZnSe_{0.22}S_{0.78}$, and Mn:ZnS QDs show the onset of temperature quenching of PL around 380, 400, 460, and 480 K; and after heating to 500 K, the PL intensity drops off 58%, 32%, 13%, and 5%, respectively, compared to that at 300 K. The temperature dependence of the luminescence intensity can be described by an Arrhenius equation:[19,38]

$$I(T) = \frac{I_0}{1 + Ae^{-\Delta E/k_B T}} \quad (1)$$

where $I_0$ is the initial PL intensity, $I(T)$ is the intensity at different temperatures, $\Delta E$ is activation energy of thermal quenching, $A$ is a constant for a certain host, and $k_B$ is the Boltzmann constant. The solid lines in Fig. 5 represent a simulation of the intensities using this equation, which fit well with the experimental results, suggesting that the thermally activated escape of charge carriers can explain the decrease in PL intensity. The activation energy is about 0.37, 0.48, 0.65, and 0.92 eV for the Mn:ZnSe, $Mn:ZnSe_{0.73}S_{0.27}$, $Mn:ZnSe_{0.22}S_{0.78}$, and Mn:ZnS QDs, respectively. The activation energies rise with increasing the host bandgap. This clearly demonstrates the role of host bandgap on the thermal stability of PL in Mn-doped QDs with wide bandgap, such as ZnS or a $ZnSe_{0.22}S_{0.78}$ alloy, eliminating the thermally activated escape of carriers to the host by the large activation energies, thus improving the high temperature optical performance of Mn-doped QDs. Further, we notice that the thermal activation energy is much larger than the thermal energy of $k_BT$, it seems that the thermal activation process is inefficient. However, the inefficient nonradiative processes may reduce the PL QY because of the very small $Mn^{2+}$ ion radiative transition rate constant.[37,39]

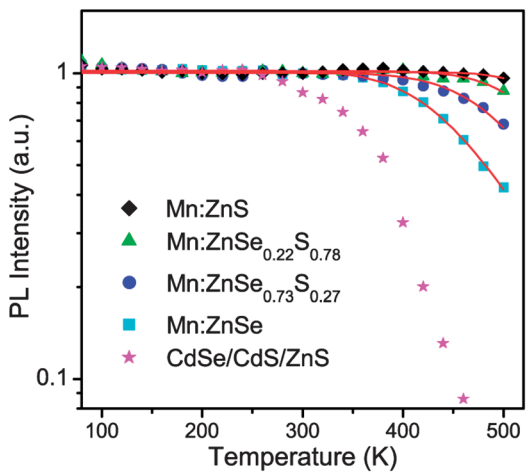


Fig. 5 The integrated PL intensities of Mn:ZnS (black rhombuses), $Mn:ZnSe_{0.22}S_{0.78}$ (green triangles), $Mn:ZnSe_{0.73}S_{0.27}$ (blue circles), Mn:ZnSe (cyan squares), and CdSe–CdS–ZnS (magenta stars) core–shell QDs at different temperatures from 80 to 500 K, under excitation at 280 nm. The red solid lines represent fitting curves using eqn (1).

It is exciting to see that four different highly efficient Mn-doped QD systems all possess high luminescence quenching temperatures (defined as the temperature at which the emission reaches half of its maximum intensity) over 200 °C, higher than Mn-doped nanocrystals and workhorse CdSe QDs reported so far. The factors resulting in the low quenching temperatures of Mn-doped QDs reported before have been discussed in the above. For the pristine CdSe QDs, we plot the integrated PL intensity of CdSe–CdS–ZnS core–shell QDs with a high luminescence QY (67%) as a function of temperature in Fig. 5, corresponding PL spectra are shown in the ESI (Fig. S4).† The undoped CdSe QDs have a quenching temperature of about 100 °C, much lower than our Mn-doped QDs. The great difference between the quenching temperatures of the undoped and Mn-doped QDs can be understood by the different emission mechanisms for the two cases. For the undoped QDs, the emission arises from the direct recombination of the exciton; while for the Mn-doped QDs, the emission is attributed to the $Mn^{2+}$ ion d–d transition, which is excited by the host exciton energy transfer.[39,40] The fast energy transfer process (a few to tens of picoseconds)[28,29] will effectively compete with nonradiative decay by trap states, which makes $Mn^{2+}$ ion emission more robust than exciton luminescence in undoped QDs.[41] Furthermore, the d-electrons are almost localized in the $Mn^{2+}$ ion and do not spread over the entire nanocrystal,[40] thus the $Mn^{2+}$ ion emission is less sensitive to nonradiative decay channels on the QD surface. Therefore, the Mn-doped QDs exhibit better PL thermal stability than the undoped QDs, and $Mn^{2+}$ ion doping can become a way to enhance the PL thermal stability of QDs.

For practical applications, the thermal stability of the structure is also an important factor for the QDs to be used at elevated temperature, because the thermally induced structural changes can give rise to the formation of surface states or defects.[20] The PL quenching arising from the structural changes is irreversible, which distinguishes from the reversible quenching caused by thermal activation. We recorded the temperature-dependent PL spectra and PL decay curves of Mn:ZnS QDs with different shell thickness and Mn:ZnSe QDs in heating–cooling cycle processes (Fig. S5, ESI†), and plotted the corresponding integrated PL intensities and PL lifetimes in Fig. 6. The irreversible quenching process was present in Mn-doped QDs with a thin shell, as seen in Fig. 6a. There is about 18% permanent loss of intensity after the heating and cooling cycle, accompanied by 13% permanent shortening of lifetime. The permanent drop in both PL intensity and lifetime gives evidence for the irreversible structural change in the thin shell coated Mn:ZnS QDs. Interestingly, in Mn-doped

 

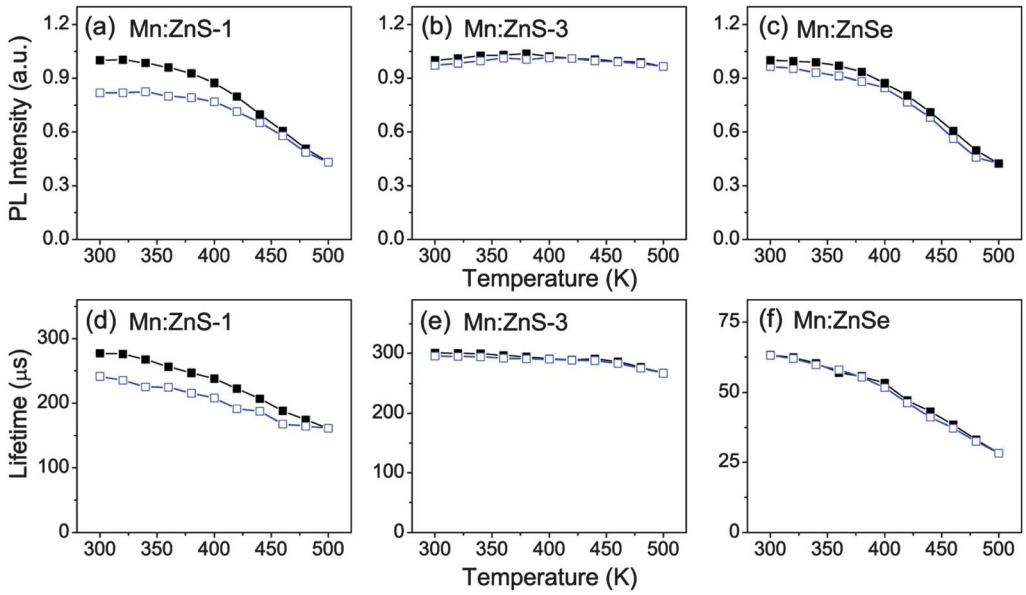


Fig. 6 Temperature-dependent integrated PL intensities (top) and decay times (bottom) of Mn:ZnS-1 (3.4 ML ZnS) (a and d), Mn:ZnS-3 (6.4 ML ZnS) (b and e), and Mn:ZnSe QDs (c and f) QDs. Black solid squares refer to the heating processes, while blue open squares represent the cooling processes.

QDs with a thick shell, such as Mn:ZnS with 6.4 ML ZnS and Mn:ZnSe with 6.2 ML ZnSe shells, both the PL intensity and lifetime almost fully recover upon cooling, which suggests that the irreversible quenching process is absent, as seen in Fig. 6b and c. Similar behavior is also present in Mn:ZnSeS QDs with a thick shell (Fig. S6, ESI†). The results mean that irreversible quenching at high temperature is not inevitable, which depends on the shell structure. The density of thermally induced surface states or traps is larger for thin shell QDs, which may be attributed by the smaller size, and the thick shell can efficiently suppress the effect of thermally created surface states on the $Mn^{2+}$ ion emission. Besides, the PL intensity drop of CdSe QDs is only partly reversible, 45% permanent loss of intensity is observed (Fig. S6, ESI†). This indicates that $Mn^{2+}$ ion emission is more robust than exciton luminescence in CdSe QDs, consistently with that the $Mn^{2+}$ ion emission is less susceptible to the trap states.

The temperature dependence of the PL peak energies for Mn:ZnS QDs with different shell thickness and Mn:ZnSe QDs in the heating–cooling cycle processes are shown in Fig. 7a. The PL peak of $Mn^{2+}$ ions is observed to gradually shift to higher energy as the temperature increases from 80 to 500 K, which is generally attributed to the thermal expansion of the host lattice decreasing crystal field strength,[19] similar to the temperature behavior of $Mn^{2+}$ ion emission in bulk semiconductors.[42] Upon cooling to 300 K, the shift is totally reversible for thick shell coated QDs, which indicates that no structure change occurs near the $Mn^{2+}$ ions, because the structure change will induce the variation in the ligand field. The results also suggest that the $Mn^{2+}$ ions do not diffuse during our experiments, because the ligand field splitting progressively increases from the core to the surface,[15] while a permanent red shift is found in the thin shell QDs, which may be caused by the increase of surface defect state emission (as seen in Fig. S5, ESI†). On the other hand, the full widths at the half-maximum (FWHM) of these QDs broaden with increasing the temperature, as seen in Fig. 7b. The temperature dependence of the bandwidth can be written as:[43]

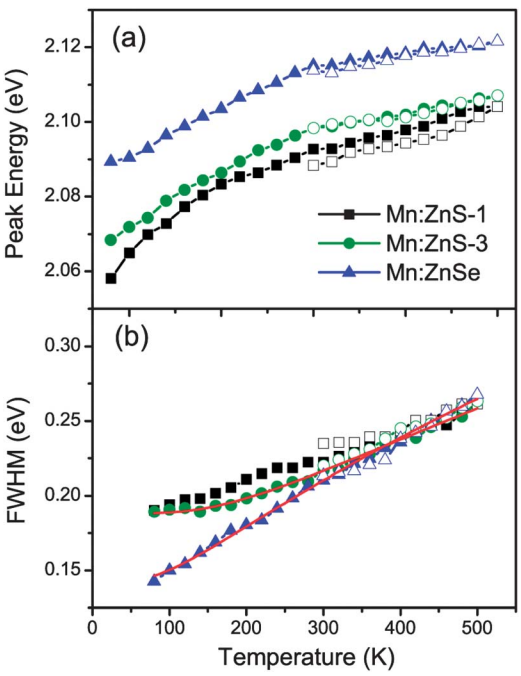


Fig. 7 Temperature dependence of emission peak energy (a) and FWHM (b) of Mn:ZnS-1 (3.4 ML ZnS, black squares), Mn:ZnS-3 (6.4 ML ZnS, green circles), and Mn:ZnSe (blue triangles) QDs. The solid symbols refer to heating processes, the open symbols represent cooling processes. The red solid lines represent fitting curves using eqn (2).

$$\Gamma(T) = \Gamma_0 \sqrt{\coth\left(\frac{\hbar\omega}{2k_B T}\right)} \quad (2)$$

Here $\Gamma_0$ is the bandwidth at 0 K and $\hbar\omega$ is the energy of the lattice vibration (or phonon) that couples with the electronic transition. The bandwidth as a function of temperature can be fitted well by eqn (2), as seen by the red solid curves in Fig. 7b. The parameters $\hbar\omega$ are obtained to be 46 and 28 meV for Mn:ZnS and Mn:ZnSe QDs, respectively, similar to the values reported for bulk Mn:ZnS (41 meV) and Mn:ZnSe (31 meV),[43,44] the small difference may be caused by the strain at the core–shell interface.[45] The variation in bandwidth at high temperature is reversible for thick shell QDs, while irreversible for the thin shell ones, as seen in Fig. 7b, which confirms that the thick shell can efficiently suppress the effect of thermal creation surface states on the $Mn^{2+}$ ion emission.

## 4. Conclusions

In summary, we have studied the thermal stability of $Mn^{2+}$ ion emissions in Mn-doped core–shell QDs with different shell structures at the temperature ranging from 80 to 500 K. By comparing the temperature-dependent PL intensity and lifetime, the thermal quenching of highly efficient Mn-doped QDs is mainly caused by the thermally activated escape of carriers from the excited $Mn^{2+}$ ions, which presented at elevated temperature and can be controlled by the shell thickness and the host bandgap. The thermal stability of $Mn^{2+}$ ion emission can be improved by increasing the shell thickness, reducing the density of nonradiative recombination centers, making the $Mn^{2+}$ ions sufficiently far away from the surface traps, and enhancing the host bandgap. The highly efficient Mn:ZnSe, Mn:ZnSeS, and Mn:ZnS QDs with thick shells possessed high PL quenching temperature over 200 °C; excitingly, the Mn:ZnS QDs kept a high PL QY ~50% even at 500 K. Further, the Mn-doped QDs exhibited excellent thermal robustness in the heating–cooling experiments, better than pristine CdSe core–shell QDs. The PL intensity, peak energy, and FWHM for thick shell coated Mn-doped QDs can almost completely recover after heating up to 500 K. Therefore, heavy metal-free Mn-doped QDs are promising to be used in high-efficiency and environmentally safe QD optical devices, in which the strong thermal effects are inevitable.

## Acknowledgements

This work was supported by the National Natural Science Foundation of China (no. 11274304, and 11204298, 61106066, 61205025, and 21101038). We thank Mr Rong'an Shen for his help in the preparation of Mn-doped QDs.

## Notes and references

1 S. Coe, W. K. Woo, M. G. Bawendi and V. Bulović, *Nature*, 2002, **420**, 800–803.
2 Y. Shirasaki, G. J. Supran, M. G. Bawendi and V. Bulović, *Nat. Photonics*, 2013, **7**, 13–23.
3 A. G. Pattantyus-Abraham, I. J. Kramer, A. R. Barkhouse, X. H. Wang, G. Konstantatos, R. Debnath, L. Levina, I. Raabe, M. K. Nazeeruddin, M. Grätzel and E. H. Sargent, *ACS Nano*, 2010, **4**, 3374–3380.
4 K. Dohnalová, A. N. Poddubny, A. A. Prokofiev, W. D. Boer, C. P. Umesh, J. M. Paulusse, H. Zuilhof and T. Gregorkiewicz, *Light: Sci. Appl.*, 2013, **2**, e47.
5 P. K. Santra and P. V. Kamat, *J. Am. Chem. Soc.*, 2012, **134**, 2508–2511.
6 H. Yang and P. H. Holloway, *J. Phys. Chem. B*, 2003, **107**, 9705–9710.
7 H. Yang, P. H. Holloway and B. B. Ratna, *J. Appl. Phys.*, 2003, **93**, 586–592.
8 N. Pradhan, D. M. Battaglia, Y. C. Liu and X. G. Peng, *Nano Lett.*, 2007, **7**, 312–317.
9 A. R. Maity, S. Palmal, S. K. Basiruddin, N. S. Karan, S. Sarkar, N. Pradhana and N. R. Jana, *Nanoscale*, 2013, **5**, 5506–5513.
10 S. Cao, J. J. Zheng, J. L. Zhao, L. Wang, F. M. Gao, G. D. Wei, R. S. Zeng, L. H. Tian and W. Y. Yang, *J. Mater. Chem. C*, 2013, **1**, 2540–2547.
11 W. J. Zhang, Y. Li, H. Zhang, X. G. Zhou and X. H. Zhong, *Inorg. Chem.*, 2011, **50**, 10432–10438.
12 R. S. Zeng, M. Rutherford, R. G. Xie, B. S. Zou and X. G. Peng, *Chem. Mater.*, 2010, **22**, 2107–2113.
13 N. Pradhan and X. G. Peng, *J. Am. Chem. Soc.*, 2007, **129**, 3339–3347.
14 R. S. Zeng, T. T. Zhang, G. Z. Dai and B. S. Zou, *J. Phys. Chem. C*, 2011, **115**, 3005–3010.
15 A. Hazarika, A. Layek, S. De, A. Nag, S. Debnath, P. Mahadevan, A. Chowdhury and D. D. Sarma, *Phys. Rev. Lett.*, 2013, **110**, 267401.
16 D. J. Norris, N. Yao, F. T. Charnock and T. A. Kennedy, *Nano Lett.*, 2001, **1**, 3–7.
17 W. Chen, A. G. Joly, J. Malm, J. Bovin and S. P. Wang, *J. Phys. Chem. B*, 2003, **107**, 6544–6551.
18 M. Tanaka and Y. Masumotoa, *Chem. Phys. Lett.*, 2000, **324**, 249–254.
19 W. Chen, F. H. Su, G. H. Li, A. G. Joly, J. Malm and J. Bovin, *J. Appl. Phys.*, 2002, **92**, 1950–1955.
20 Y. M. Zhao, C. Riemersma, F. Pietra, R. Koole, C. M. Donegá and A. Meijerink, *ACS Nano*, 2012, **6**, 9058–9067.
21 V. Bachmann, C. Ronda and A. Meijerink, *Chem. Mater.*, 2009, **21**, 2077–2084.
22 J. J. Zheng, X. Yuan, M. Ikezawa, P. T. Jing, X. Y. Liu, Z. H. Zheng, X. G. Kong, J. L. Zhao and Y. Masumoto, *J. Phys. Chem. C*, 2009, **113**, 16969–16974.
23 J. S. Park, S. W. Mho, J. C. Choi, H. L. Park, G. C. Kim, S. H. Lee and J. S. Kim, *J. Korean Phys. Soc.*, 2007, **50**, 571–574.
24 F. H. Su, B. S. Ma, Z. L. Fang, K. Ding, G. H. Li and W. Chen, *J. Phys.: Condens. Matter*, 2002, **14**, 12657–12664.
25 Y. G. Yang, O. Chen, A. Angerhofer and Y. C. Cao, *Chem.–Eur. J.*, 2009, **15**, 3186–3197.
26 N. Pradhan and D. D. Sarma, *J. Phys. Chem. Lett.*, 2011, **2**, 2818–2826.
27 R. Beaulac, P. I. Archer, S. T. Ochsenbein and D. R. Gamelin, *Adv. Funct. Mater.*, 2008, **18**, 3873–3891.

 

28 H.-Y. Chen, S. Maiti and D. H. Son, *ACS Nano*, 2012, **6**, 583–591.
29 Y. Hefetz, W. C. Goltsos, A. V. Nurmikko, L. A. Kolodziejski and R. L. Gunshor, *Appl. Phys. Lett.*, 1986, **48**, 372–374.
30 F. V. Mikulec, M. Kuno, M. Bennati, D. A. Hall, R. G. Griffin and M. G. Bawendi, *J. Am. Chem. Soc.*, 2000, **122**, 2532–2540.
31 S. C. Erwin, L. J. Zu, M. I. Haftel, A. L. Efros, T. A. Kennedy and D. J. Norris, *Nature*, 2005, **436**, 91–94.
32 H. Menkara, R. A. Gilstrap, Jr, T. Morris, M. Minkara, B. K. Wagner and C. J. Summers, *Opt. Express*, 2011, **19**, 972–981.
33 B. Yang, J. Zhang, Y. Cui and K. Wang, *Appl. Opt.*, 2011, **50**, 137–141.
34 D. Valerini, A. Cretí, M. Lomascolo, L. Manna, R. Cingolani and M. Anni, *Phys. Rev. B: Condens. Matter Mater. Phys.*, 2005, **71**, 235409.
35 P. T. Jing, J. J. Zheng, M. Ikezawa, X. Y. Liu, S. Z. Lv, X. G. Kong, J. L. Zhao and Y. Masumoto, *J. Phys. Chem. C*, 2009, **113**, 13545–13550.
36 E. J. McLaurin, V. A. Vlaskin and D. R. Gamelin, *J. Am. Chem. Soc.*, 2011, **133**, 14978–14980.
37 V. A. Vlaskin, N. Janssen, J. V. Rijssel, R. Beaulac and D. R. Gamelin, *Nano Lett.*, 2010, **10**, 3670–3674.
38 D. Valerini, A. Cretí, M. Lomascolo, L. Manna, R. Cingolani and M. Anni, *Phys. Rev. B: Condens. Matter Mater. Phys.*, 2005, **71**, 235409.
39 R. Beaulac, P. I. Archer and D. R. Gamelin, *J. Solid State Chem.*, 2008, **181**, 1582–1589.
40 K. P. Kadlag, M. J. Rao and A. Nag, *J. Phys. Chem. Lett.*, 2013, **4**, 1676–1681.
41 H.-Y. Chen and D. H. Son, *Isr. J. Chem.*, 2012, **52**, 1016–1026.
42 G. Morello, M. Anni, P. D. Cozzoli, L. Manna, R. Cingolani and M. D. Giorgi, *J. Phys. Chem. C*, 2007, **111**, 10541–10545.
43 J. F. Suyver, J. J. Kelly and A. Meijerink, *J. Lumin.*, 2003, **104**, 187–196.
44 W. C. Zhou, R. B. Liu, D. S. Tang, X. X. Wang, H. M. Fan, A. Pan, Q. L. Zhang, Q. Wan and B. S. Zou, *Nanotechnology*, 2013, **24**, 055201.
45 H.-Y. Chen, S. Maiti, C. A. Nelson, X. Y. Zhu and D. H. Son, *J. Phys. Chem. C*, 2012, **116**, 23838–23843.